Visible ruthenium particles were not observed during STEM examination of these catalysts. The highly dispersed nature of ruthenium in these catalysts was further supported by gas adsorption measurements, which resulted in H_2:Ru = 0.85 and O:Ru = 0.87 for Catalyst 4956-86 and H_2:Ru and O:Ru = 1.1 for Catalyst 4966-72. These H_2 and O uptakes were significantly higher than those obtained with other alumina-supported catalysts having 4-6 nm ruthenium particles. Catalyst 4966-72 was also examined by EXAFS which indicated the average ruthenium particle size to be 0.8 nm.

The H_2:Ru ratio was 0.13 while the O:Ru ratio was 0.48 for titania-supported Catalyst 5345-61. The low H_2 uptake on this catalyst after oxygen exposure at room temperature may be possibly explained by migration of titania over ruthenium. The higher oxygen uptake relative to the uptake of hydrogen may be explained if most of the oxygen adsorbs on titania.

5.1.5 Application of EXAFS to Characterization of Ruthenium Catalysts

5.1.5.1 Measurements at CHESS

The first series of experiments were conducted at the Cornell High Energy Synchrotron Source (CHESS). The ruthenium catalysts that were examined were reduced and transferred to sample cells under N_2 in a glove bag. A rereduction step was not performed prior to these EXAFS measurements. The catalysts that were examined were: Catalyst 4956-76 after use in Run 15 and fresh Catalysts 4956-101, 4966-76 and 4966-72. Also, a physical mixture of ruthenium metal powder and γ-Al_2O_3 (1% Ru) was analyzed.

In a previous literature report on Ru catalysts, it was demonstrated that even very low oxygen concentrations applied at room temperature lead to disruption of small Ru particles [71]. Similar reports have been made for Pt and Rh

for the adsorption of CO and O_2 [72,73]. The first series of catalysts fall naturally into two groups: those with large ruthenium particles which are resistant to disruption by oxygen and those sensitive to oxygen disruption. Used Catalyst 4956-76 is unequivocally insensitive to oxygen disruption while Catalyst 4956-101 originally contained both smaller particles which were disrupted and larger particles which remained intact. Fresh Catalysts 4966-76 and 4966-72 undoubtedly consisted of smaller particles, few of which survived the measurement conditions.

These observations can be made simply by looking at the extracted Chi function even without performing a Fourier transform. Figures 5-79 through 5-83 show the Chi functions for the five samples examined. From the Ru metal and used catalyst sample, it is clear that metallic Ru EXAFS is characterized by oscillations with maximum amplitude in the vicinity of $k=10\text{Å}^{-1}$. The Chi of fresh Catalyst 4966-72 is more representative of oxidized Ru with very large amplitude oscillations near the origin of the Chi function which rapidly and monotonically damps to near zero amplitude at about $k=10\text{Å}^{-1}$. For those species in between, a superposition of the two EXAFS types can be seen. (Even for the most oxidized sample, some evidence for larger Ru particles is evident in the Chi function.)

In light of the method for determining particle size, no analysis is possible for Catalysts 4966-76 and 4966-72. Since only part of the Ru in Catalyst 4956-101 is in the form of relatively large Ru particles, further clarification of the method for determining particle size is required. In the present case, some of the Ru is in an oxidized state and will not contribute to the metallic coordination numbers. Thus, since a sample average coordination number is being derived, the absolute coordination numbers must be smaller than the pure metallic phase, no matter what the actual particle size. By using the

Figures 5-79 through 5-83. EXAFS Chi Function for Measurements at CHESS

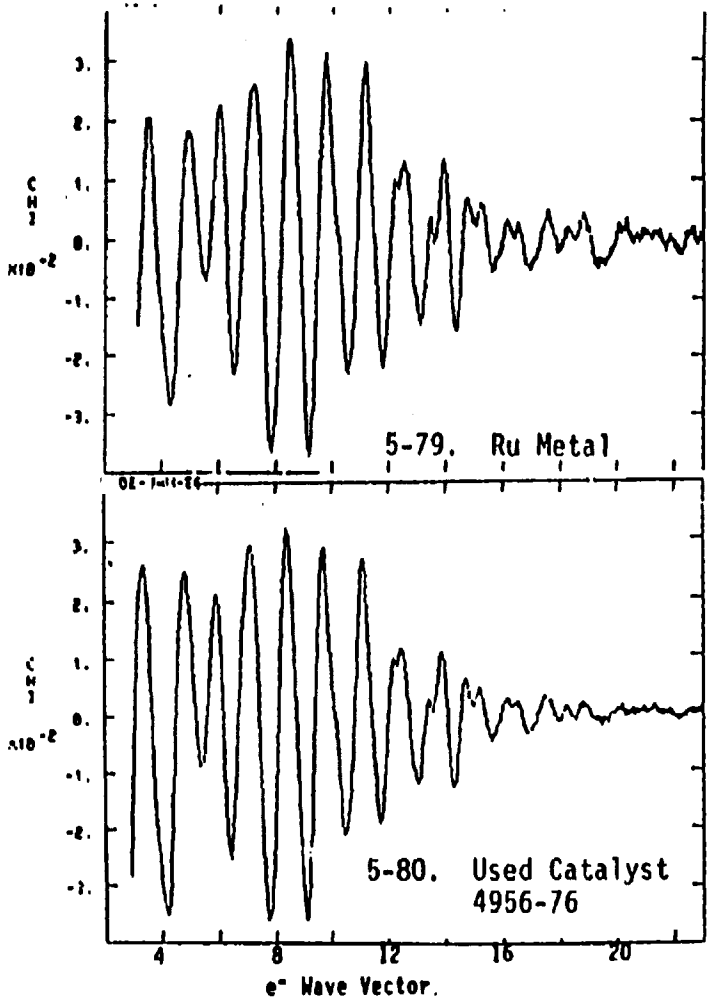

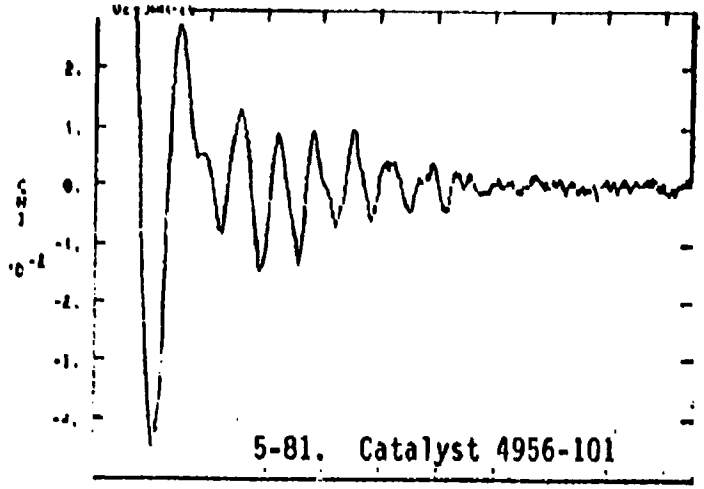

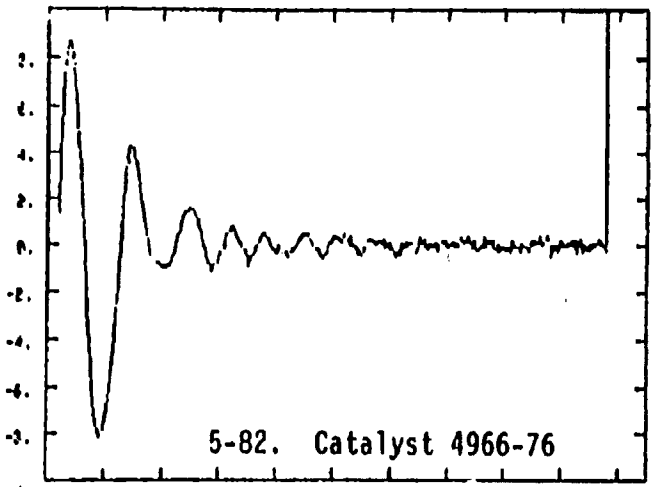

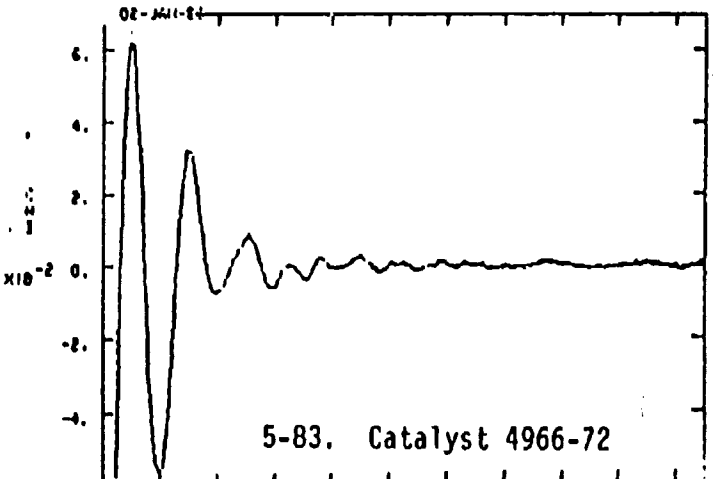

scale of relative apparent coordination numbers, the drop-off in observed coordination number can be scaled rigidly by a single multiplicative constant in order to determine size and estimate the fraction in the metallic state.

Figures 5-84 through 5-88 show the k-weighted Fourier transforms of the Chi data. The similarity in shell structure is readily apparent in the samples containing metallic ruthenium particles. The shells selected for analysis were 1+2, 3, and 8. Other intermediate shells are too convoluted with one another to afford a reliable separation into a single shell contribution. Table 5-16 lists

Table 5-16

Fitting Parameters for Ru Catalysts from EXAFS Measurements at CHESS

Sample	Shell	Relative Coordination Number	Distance (Å)
Used 4956-76	1+2	1.15	2.678
	3	1.06	3.794
	8	1.19	5.413
4956-101	1+2	0.40	4.684
	3	0.32	3.791
	8	0.33	5.413

the apparent relative coordination numbers for used Catalysts 4956-76 and 4956-101. Based on these trends and on the curve in Figure 4-3, the following conclusions can be made:

1) Most of the Ru in used Catalyst 4956-76 is in crystallites greater than 4 nm.

2) Approximately one-third of the Ru in Catalyst 4956-101 remains in the metallic state, with a particle size of about 4 nm.

Figures 5-84 through 5-88. Fourier Transforms for EXAFS Measurements at CHESS

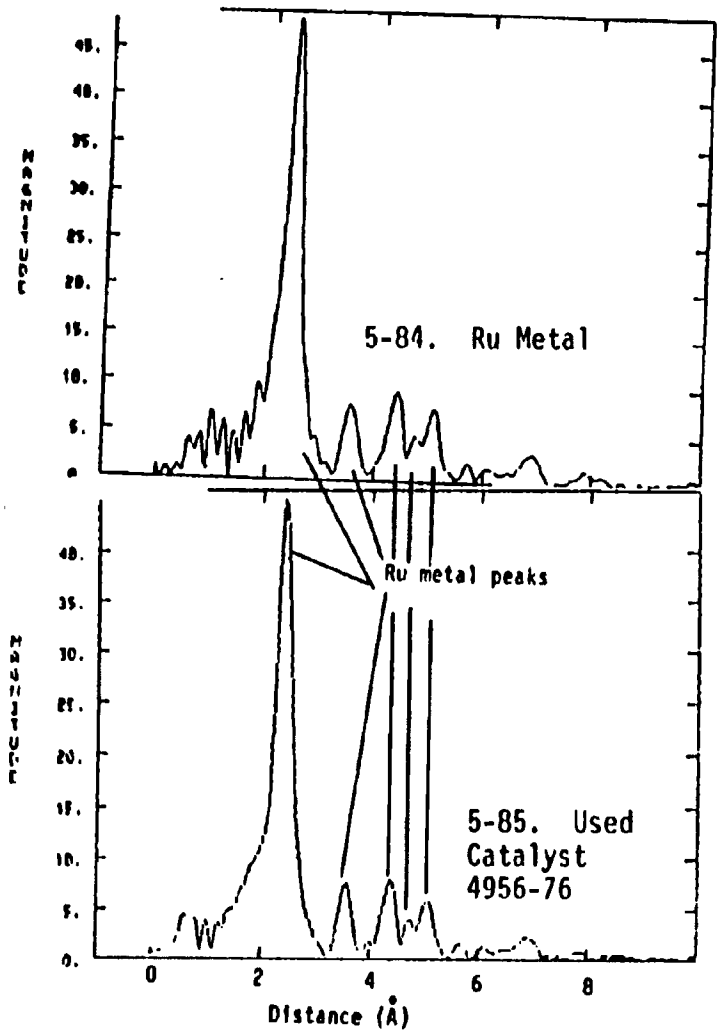

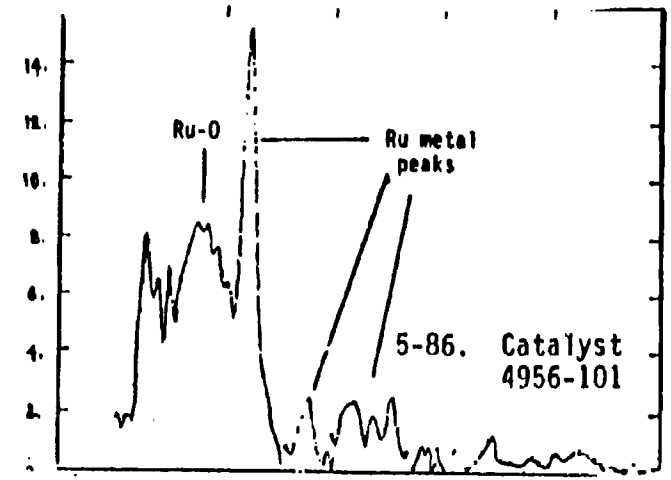

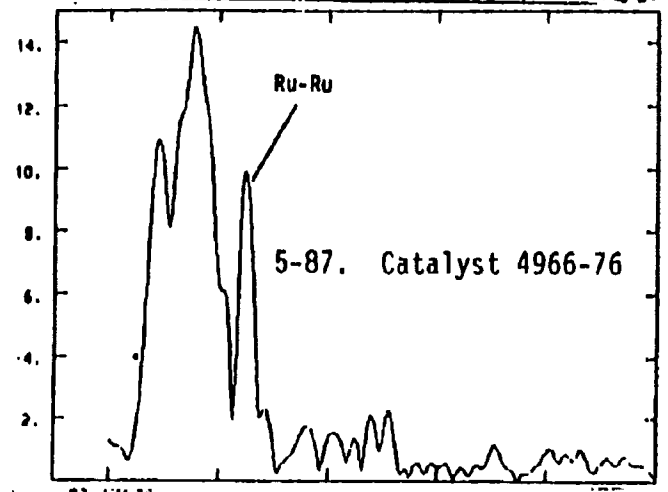

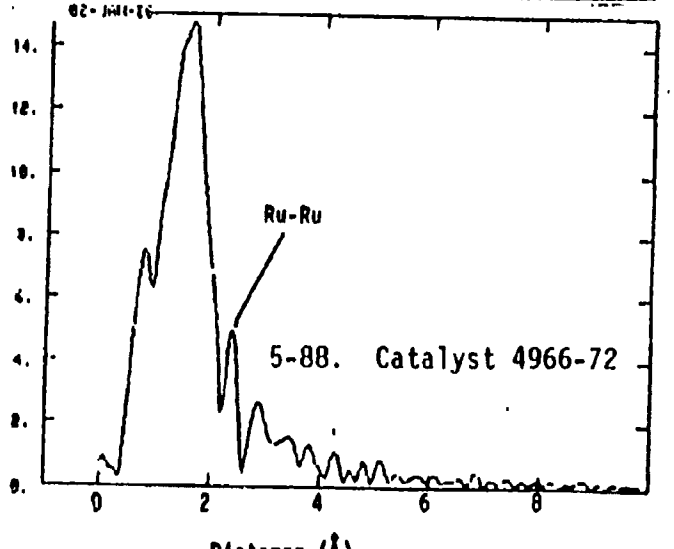

The fraction of Ru in sample 3 in the metallic state derives from the multiplicative factor needed to bring the relative coordination numbers onto the same scale as the used Catalyst 4956-76. Even though the metallic Ru sample was annealed, it appears not to be nearly as good a standard for Ru metal as the spent catalyst itself. This is reflected in the cleaner Fourier transform and the apparent coordination numbers so consistently higher than 1.0 by about 12%.

For the remaining samples, some qualitative comments can be made regarding the original distribution of sizes. The susceptibility of the Ru particles to disruption by oxygen decreases with increasing particle size. It is not unlikely that particles in the range of 2 nm will oxidize on the surface and lead to a misregistry of the outermost Ru atoms, but leave the interior of the particle intact as an apparently smaller Ru crystallite. By using a combination of qualitative arguments, a ranking of original size distributions can still be made. Even in Catalyst 4966-72, which is the most oxidized, some evidence for a Ru-Ru nearest neighbor feature can be seen. This feature decreases in size in the order of the samples given: 4956-101, 4966-76, 4966-72. Since Catalyst 4956-101 can be analyzed for size in the conventional way, it can be used as a reference point. Clearly, the Ru-O feature in this catalyst is smaller than in either Catalyst 4966-76 or 4966-72. It was argued above that about 1/3 of the Ru remained in metallic particles in Catalyst 4956-101. This then requires that the amplitude of the Ru-O feature represent around 2/3 of the Ru. This is quite consistent with the Ru-O features found in Catalysts 4966-76 and 4966-72. Assuming the same chemical species in all of the samples, the Ru-O peak in Catalysts 4966-76 and 4966-72 should represent nearly all of the Ru species. However, in light of the residual Ru-Ru features, Catalyst 4966-76 originally had larger Ru particles than Catalyst 4966-72.

The single factor most influencing the viability of crystallite size determination by EXAFS in this investigation was the disruption of Ru particles by exposure to oxygen. Despite the conventional precautions against air exposure, impurities of oxygen in purge gases or even the slightest intrusion at any point in sample handling clearly leads to oxidation of the smallest metal particles. Whether the nature of the oxidized species is the same as found in the bulk oxide is of little relevance here. Even chemisorption of oxygen, if it results in changes in particle morphology, is a detrimental oxidation. These effects must be present in all samples studied *ex situ* by any technique.

5.1.5.2 Measurements at Brookhaven National Laboratory

Accordingly, the second series of catalysts were reduced *in situ* prior to EXAFS measurements. These data were taken at Brookhaven National Laboratory on beamline X-18B. Fluorescence detection was used rather than transmission. The catalysts that were examined were fresh Catalysts 4966-72, 4966-96-2, 4966-76, 4966-114, 4966-106, 4966-102, Catalyst 4966-72 after use in Run 18 and ruthenium metal powder - γ-Al_2O_3 physical mixture.

The background removed, normalized EXAFS Chi functions observed are shown in Figures 5-89 through 5-96. The associated k weighted Fourier transforms are given in Figure 5-97. A number of qualitative observations can be made simply by examining the Chi functions in Figures 5-89 through 5-96. The amplitudes of the oscillations can be seen to vary substantially between catalyst samples. Catalyst 4966-102 and the used Catalyst 4966-72 have Chi functions which are similar to the Ru metal standard. For the two samples which have much smaller amplitude oscillations, Catalyst 4966-72 and Catalyst 4966-96-2, the oscillations extend over the entire range of k without significant loss of amplitude. This indicates that the particles, though small, are relatively well ordered.

Figures 5-89 through 5-92. EXAFS Chi Function for Measurements at Brookhaven National Laboratory

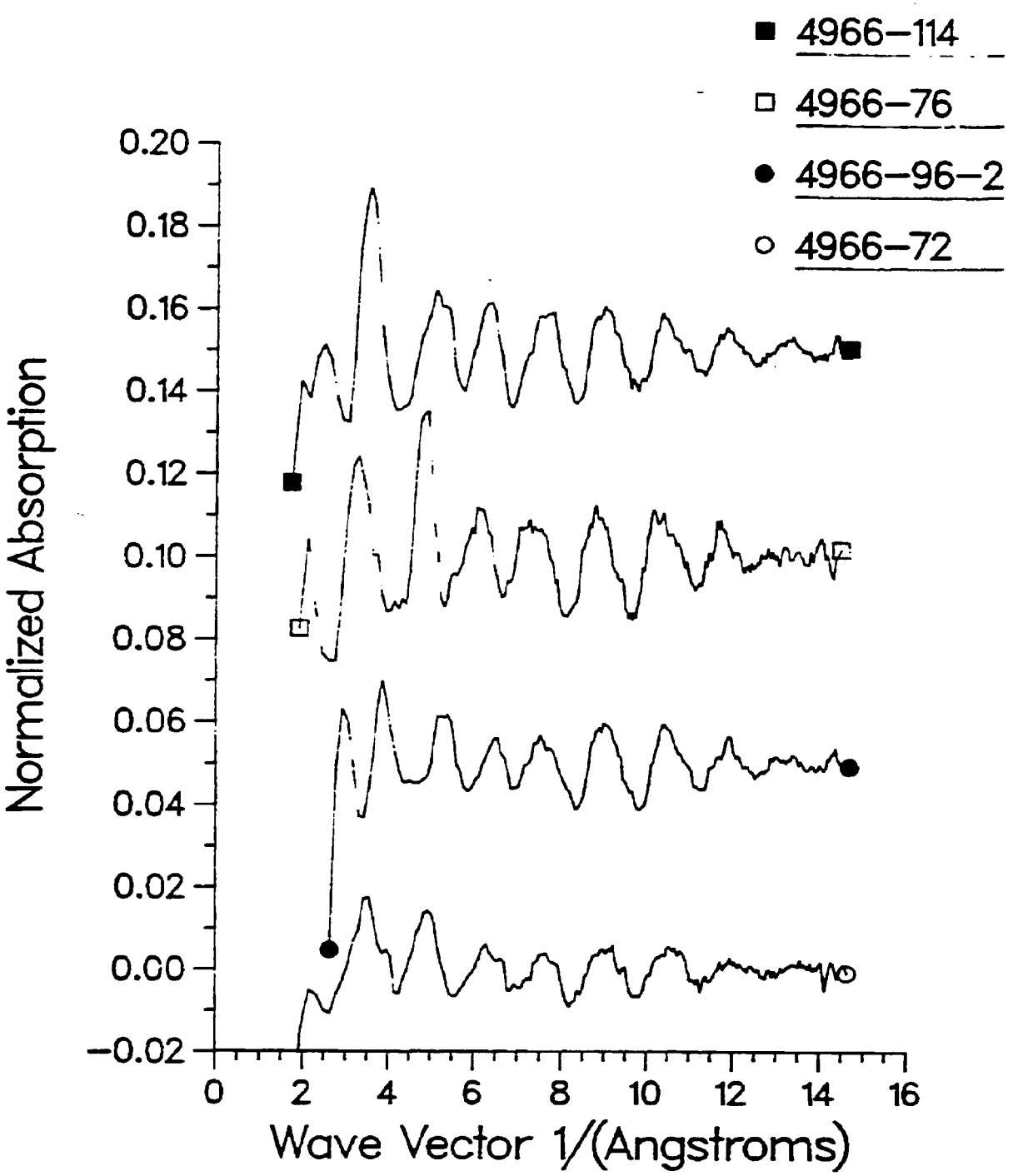

Figures 5-93 through 5-96. EXAFS Chi Function for Measurements at Brookhaven National Laboratory

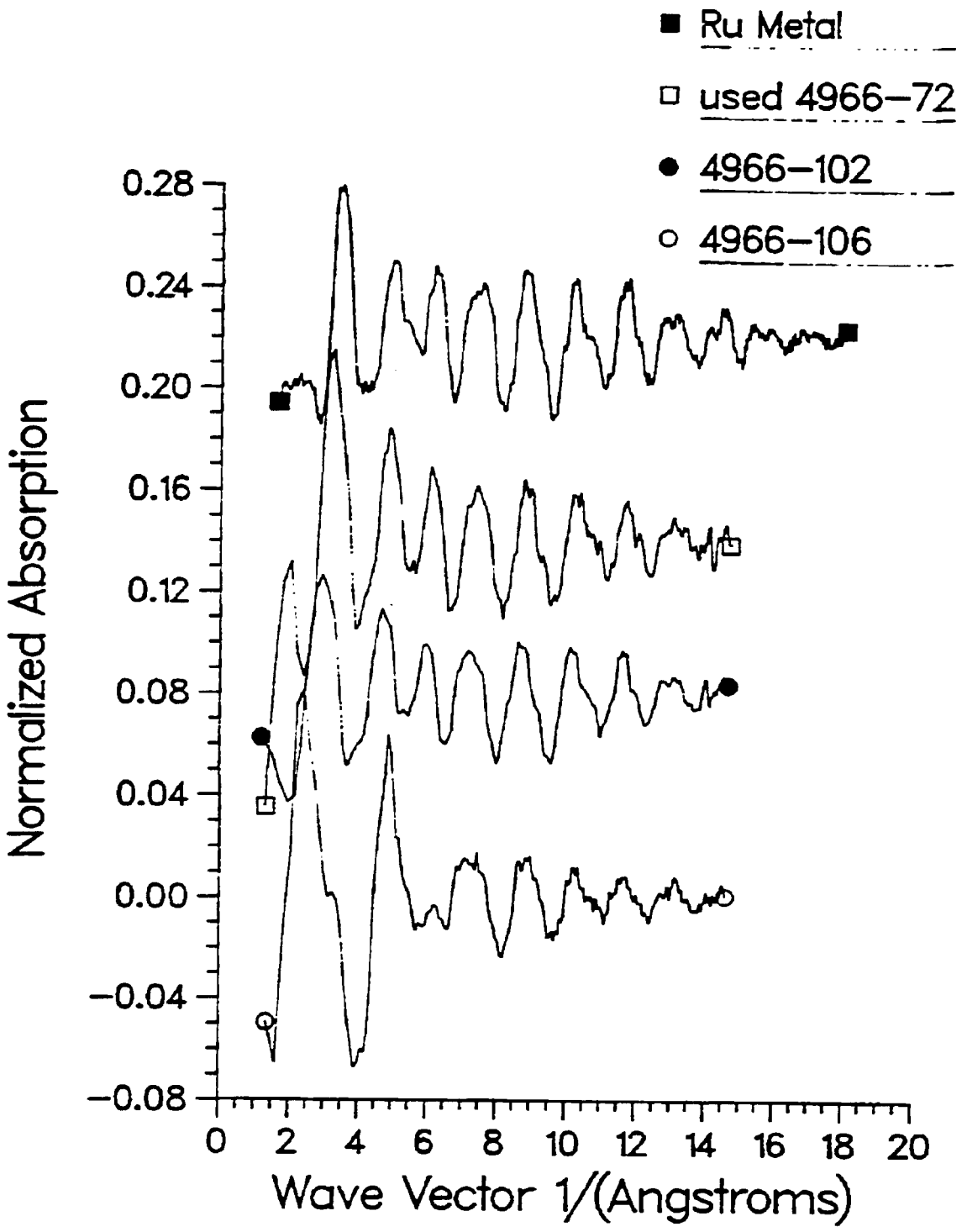

Figure 5-97a. Fourier Transforms for EXAFS Measurements at Brookhaven National Laboratory

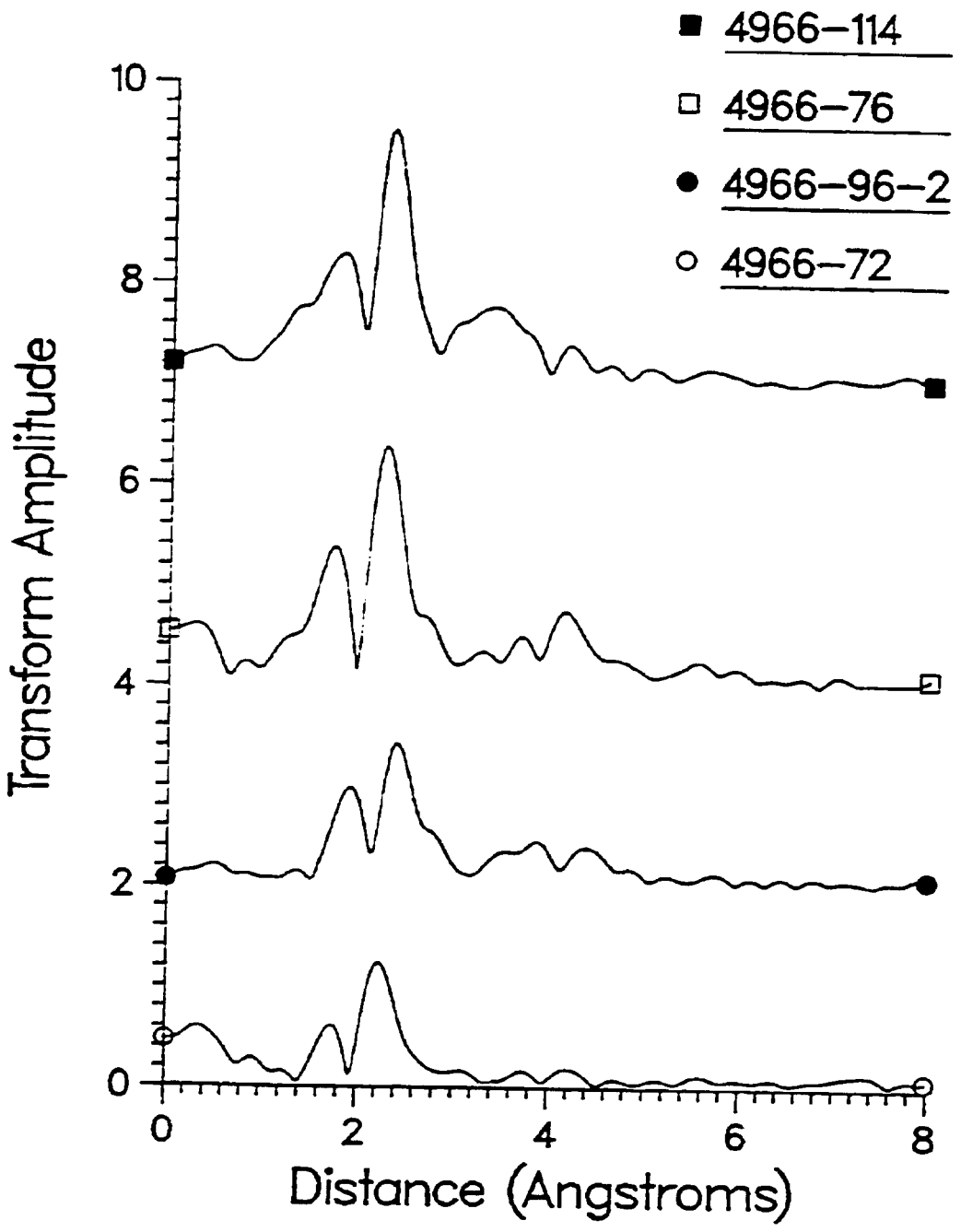

Figure 5-97b. Fourier Transforms for EXAFS Measurements at Brookhaven National Laboratory

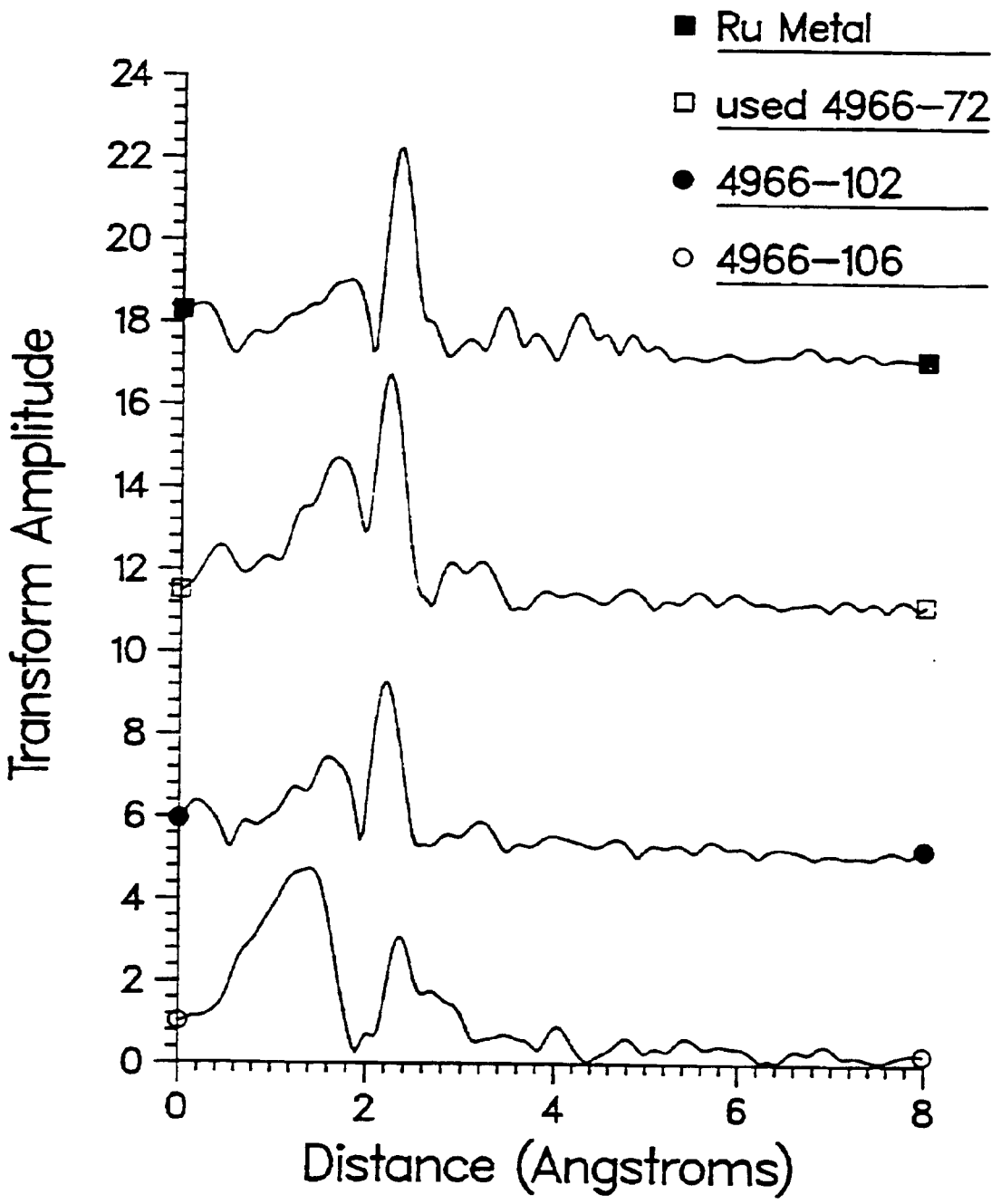

Examining Catalyst 4966-106, the strong extra oscillations at low k are characteristic of Ru-O interaction, immediately suggesting that the reduction procedure used results only in partial reduction. However, the particles which are formed are relatively large, as seen by the amplitude of the oscillations seen in the region characteristic of Ru-Ru interaction.

The qualitative observations based on the raw Chi functions are also reflected in the Fourier transforms in Figure 5-97. Since there is little apparent loss of EXAFS amplitude due to disorder in these systems, the transform amplitude is a reasonable gauge of the coordination number of a given coordination shell. As expected, those catalysts with Chi similar to metallic Ru also have Fourier transforms which look like that of the metal. For catalysts with smaller particle sizes, the nearest neighbor coordination shell, as well as the more distant shells, are reduced in amplitude.

The results of curve fitting the backtransform-filtered nearest neighbor shell are given in Table 5-17. By using only the nearest neighbor coordination

Table 5-17

EXAFS Curve Fitting Results for Ru Nearest Neighbors from Measurements at Brookhaven National Laboratory

Catalyst	Bond Length (Å)	Disorder Parameter ($X10^{-3}$)	Coordination Number	Ru Particle Size
4966-72 (Fresh)	2.61	2.08	3.4	0.8 nm
4966-96-2	2.67	0.96	4.5	1-3 nm
4966-76	2.65	2.79	8.1	Bimodal Distribution 1.5-4 nm
4966-114	2.64	3.36	8.1	Narrow Distribution 1.5 nm
4966-106 (Partially Reduced)				2-3 nm
4966-102	2.66	1.30	11.9	4 nm
4966-72 (Used)	2.65	1.17	13.6	>4 nm
4956-101				Not Analyzed

numbers, a determination of the average size of the ruthenium particles can be made. However, by including qualitative observations of the highest coordination shells, information on the distribution of sizes can also be obtained. For example, fresh Catalyst 4966-72 shows a very small nearest neighbor coordination number and very small features in the Fourier transform where the higher coordination shells are expected to appear. This indicates that the vast majority of particles are indeed very small, but a few larger particles may be present. An indication of a bimodal distribution of particles sizes is found in Catalyst 4966-76. Although the nearest neighbor shell gives a relatively small coordination number, higher coordination shells appear with disproportionately large amplitude in the transform. Thus, a wide distribution of sizes is present, many of the particles are small, but there are also relatively larger ones present.

As a final sample, Catalyst 4966-114 shows a relatively low nearest neighbor coordination number with the more distant shells falling off nearly monotonically in amplitude. This is exactly what is expected for a narrow size distribution of particles.

As was pointed out above, Catalyst 4966-106 is only partially reduced. The transform shows a clear Ru-O peak at shorter distances than the Ru-Ru contribution, but also shows amplitude from higher shells. This is in keeping with a partially reduced sample with relatively large Ru particles. These results are also summarized in Table 5-17.

Catalysts 4966-72 and 4966-76 had been examined previously with EXAFS in a state where oxygen intrusion was not rigorously prevented. The results showed that the majority of the Ru had been oxidized. It is interesting to compare the results obtained for these catalysts under the two different conditions. In the present case, Catalyst 4966-72 appears to have predominantly very small Ru particles with only a small fraction present as larger assemblies. This is in good agreement with the previous result. Through exposure to oxygen, the very

small particles were oxidized while the larger particles oxidized only on their surfaces leaving an inner core of metallic Ru. Similarly for Catalyst 4966-76, the oxidized case showed both oxidized and some metallic Ru. The amount of metallic Ru for Catalyst 4966-76 was found to be larger than the Catalyst 4966-72. This is entirely consistent with the present results which indicate a bimodal distribution of particle sizes.

In addition to ruthenium, Catalyst 4966-96-2 and Catalyst 4966-102 contained K and Fe, respectively. Evidence for direct interaction between these elements and the dominant Ru is not readily apparent. In order to reveal these interactions, if they exist, it would be best to examine the K and Fe EXAFS directly. This is possible for both elements but requires a modified experimental approach.

Some comment should be made regarding the results for one additional sample which was examined both in the present and previous series, Catalyst 4956-101. In the oxidized case, it was concluded that the average particle size was in the range 2-4 nm. In the fully reduced state, an EXAFS function which is inconsistent with the remainder of the results is observed. The normalized Chi function is shown in Figure 5-98. While it is apparent at larger values of k that Ru metallic particles are present, the large derivative-like resonance at lower k values makes it difficult to analyze these data reliably. Based on the qualitative amplitude of the oscillations at higher k, the average particle size would be in the range of 2-3 nm. This is reasonably consistent with the results found in the oxidized case. However, without the inclusion of the low k region in the Fourier transform, information from higher coordination shells is severely degraded, making a complete qualitative evaluation difficult. It should be recalled that the EXAFS present here are the sums of at least 10 separate scans. Since each scan showed the same feature, a single bad data run can be ruled out.

Figure 5-98. Chi Function for EXAFS Measurements on Catalyst 4956-101

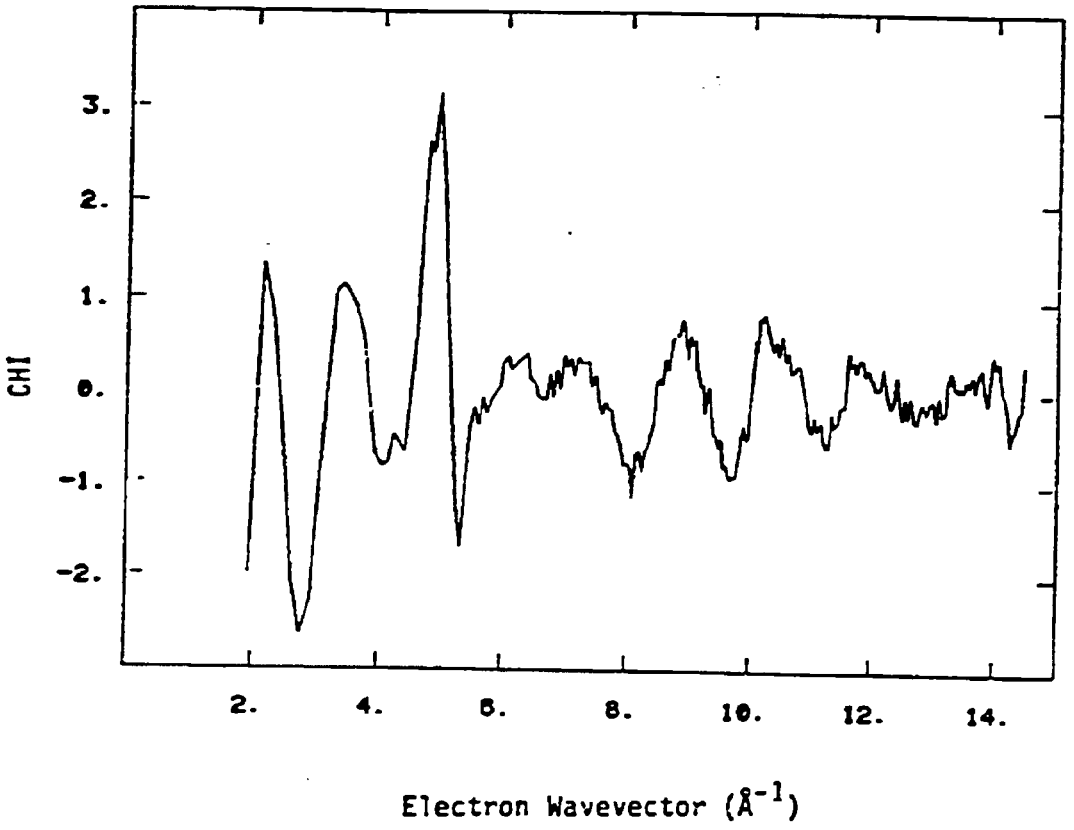

5.2 Selection of the Most Promising Catalyst Development Approach

Twenty-four runs were conducted with alumina-supported ruthenium catalysts having different size ruthenium particles in order to investigate ruthenium metal agglomeration phenomenon, hydrocarbon cutoff hypothesis and to determine ruthenium metal particle size effects in Fischer-Tropsch synthesis. Ruthenium particle size ranges that were investigated were <2 nm, ≤2-4 nm, 3-500 nm and ~5 nm. Nine runs were conducted with ruthenium catalysts supported on Y-zeolite or titania or alumina-titania in order to investigate support effects in Fischer-Tropsch synthesis. These runs are individually summarized in Sections 5.2.1 and 5.2.2. An overall analysis of these data, in the following sections, are then used for making conclusions on ruthenium metal agglomeration phenomenon, hydrocarbon cutoff hypothesis, ruthenium particle size and support effects on activity and selectivity in Fischer-Tropsch synthesis.

5.2.1 Performance of Al_2O_3-Supported Catalysts with Different Size Ruthenium Particles

5.2.1.1 Highly Dispersed Ruthenium Catalysts with ~1% Ru (by wt.)

5.2.1.1.1 Test at H_2:CO Feed Ratio = 0.9, 208°C at Inlet and 35 atm

Highly dispersed ruthenium Catalyst 4956-86 was tested in Run 16 at 208°C inlet temperature, 35 atm and 65 gas hourly space velocity (GHSV) with a feed gas having $0.9H_2$:1CO (by mole) (Tables 5-18 and 5-19 and Figures 5-99 through 5-106). The catalyst initially showed only 15% CO conversion (Figure 5-100). The space velocity was reduced to 30 GHSV after 30 hours to achieve a CO conversion of ~22%, which then gradually decreased back to ~13% by the end of the run (at 152 hours). The H_2:CO ratio at the reactor outlet was about 0.9 during the first 60 hours, decreased to about 0.8 by 90 hours, and then remained the same during the rest of the run.

Table 5-18. Product Distributions in Run 16

TOTAL PRODUCT DISTRIBUTION	
WEIGHT PCTS WITHOUT ARGON	
HYDROGEN	5.339
CARBON MONOXIDE	83.738
CARBON DIOXIDE	5.186
WATER	0.883
HYDROCARBONS	4.716
OXYGENATES	0.137
HYDROCARBON DISTRIBUTION	
C1	3.497
C2 - C4	4.518
C5 - C11	26.705
C12 - C18	15.638
C19 - C25	6.902
C26 PLUS	42.740
C1 - C44	73.237
C45 PLUS	26.763
OXYGENATES DISTRIBUTION	
ALCOHOLS	100.000
ALDEHYDES	0.000
OTHER OXYGENATES	0.000
MOLE PCTS WITHOUT ARGON	
HYDROGEN	45.346
CARBON MONOXIDE	51.187
CARBON DIOXIDE	2.018
WATER	0.839
HYDROCARBONS	0.580
OXYGENATES	0.030
RECOVERIES	
OVERALL	93.282
CARBON	94.709
HYDROGEN	102.051
OXYGEN	90.025
ARGON	98.396
CORRECTED RECOVERIES	
OVERALL	94.803
CARBON	96.254
HYDROGEN	103.715
OXYGEN	91.493

GAS ANALYSIS, WT%	
HYDROGEN	5.3392
CARBON MONOXIDE	83.7380
CARBON DIOXIDE	5.1864
METHANE	0.1649
ETHANE	0.0068
ETHYLENE	0.0128
PROPANE	0.0588
PROPYLENE	0.0214
BUTANE	0.0712
BUTENE	0.0368
AQUEOUS ANALYSIS, WT%	
WATER	0.8832
ALCOHOLS	
C1	0.0018
C2	0.0097
C3	0.0033
C4	0.0217
C5	0.1005
C6	0.0000
C7	0.0000
C8	0.0000
C9	0.0000
C10	0.0000
ALDEHYDES	
C1	0.0000
C2	0.0000
C3	0.0000
C4	0.0000
C5	0.0000
C6	0.0000
C7	0.0000
C8	0.0000
C9	0.0000
C10	0.0000
OTHER OXYGENATES	
C1	0.0000
C2	0.0000
C3	0.0000
C4	0.0000
C5	0.0000
C6	0.0000
C7	0.0000
C8	0.0000
C9	0.0000
C10	0.0000

Table 5-19. Hydrocarbon Distributions in Run 16

C1	3.4969	C51	0.6043	C101	0.1555	C151	0.0435	C201	0.0133
C2	0.4165	C52	0.5888	C102	0.1515	C152	0.0424	C202	0.0129
C3	1.7006	C53	0.5736	C103	0.1475	C153	0.0413	C203	0.0126
C4	2.4011	C54	0.5589	C104	0.1437	C154	0.0402	C204	0.0123
C5	3.2415	C55	0.5446	C105	0.1400	C155	0.0392	C205	0.0120
C6	3.3464	C56	0.5267	C106	0.1364	C156	0.0382	C206	0.0117
C7	3.6119	C57	0.5132	C107	0.1336	C157	0.0372	C207	0.0114
C8	4.2539	C58	0.5001	C108	0.1301	C158	0.0362	C208	0.0111
C9	3.8861	C59	0.4873	C109	0.1268	C159	0.0353	C209	0.0107
C10	4.8046	C60	0.4750	C110	0.1235	C160	0.0344	C210	0.0104
C11	3.5605	C61	0.4629	C111	0.1203	C161	0.0335	C211	0.0101
C12	3.1975	C62	0.4512	C112	0.1171	C162	0.0326	C212	0.0098
C13	2.8214	C63	0.4388	C113	0.1141	C163	0.0318	C213	0.0095
C14	2.4234	C64	0.4277	C114	0.1111	C164	0.0309	C214	0.0092
C15	2.0939	C65	0.4170	C115	0.1082	C165	0.0301	C215	0.0089
C16	2.0180	C66	0.4066	C116	0.1054	C166	0.0294	C216	0.0086
C17	1.6790	C67	0.3964	C117	0.1026	C167	0.0286	C217	0.0083
C18	1.4048	C68	0.3864	C118	0.1000	C168	0.0279	C218	0.0079
C19	1.1836	C69	0.3766	C119	0.0974	C169	0.0270	C219	0.0076
C20	1.0335	C70	0.3670	C120	0.0949	C170	0.0264	C220	0.0073
C21	1.2081	C71	0.3599	C121	0.0924	C171	0.0257	C221	0.0070
C22	0.8743	C72	0.3506	C122	0.0900	C172	0.0251	C222	0.0067
C23	0.8434	C73	0.3414	C123	0.0877	C173	0.0245	C223	0.0064
C24	0.8713	C74	0.3323	C124	0.0851	C174	0.0239	C224	0.0061
C25	0.8876	C75	0.3234	C125	0.0829	C175	0.0233	C225	0.0058
C26	0.8988	C76	0.3146	C126	0.0808	C176	0.0228	C226	0.0055
C27	0.9179	C77	0.3060	C127	0.0788	C177	0.0223	C227	0.0052
C28	0.9413	C78	0.2976	C128	0.0768	C178	0.0217	C228	0.0049
C29	0.9144	C79	0.2894	C129	0.0749	C179	0.0213	C229	0.0046
C30	0.9423	C80	0.2813	C130	0.0730	C180	0.0208	C230	0.0043
C31	0.8806	C81	0.2715	C131	0.0712	C181	0.0203	C231	0.0039
C32	0.9186	C82	0.2639	C132	0.0695	C182	0.0199	C232	0.0036
C33	0.8657	C83	0.2564	C133	0.0678	C183	0.0195	C233	0.0033
C34	0.8883	C84	0.2492	C134	0.0661	C184	0.0190	C234	0.0030
C35	0.7992	C85	0.2421	C135	0.0645	C185	0.0186	C235	0.0027
C36	1.0227	C86	0.2353	C136	0.0630	C186	0.0182	C236	0.0024
C37	0.7643	C87	0.2286	C137	0.0615	C187	0.0179	C237	0.0000
C38	0.9004	C88	0.2222	C138	0.0600	C188	0.0175	C238	0.0000
C39	0.7152	C89	0.2160	C139	0.0585	C189	0.0171	C239	0.0000
C40	0.8669	C90	0.2099	C140	0.0571	C190	0.0168	C240	0.0000
C41	0.7079	C91	0.2041	C141	0.0557	C191	0.0164	C241	0.0000
C42	0.7141	C92	0.1984	C142	0.0544	C192	0.0161	C242	0.0000
C43	0.6664	C93	0.1930	C143	0.0531	C193	0.0157	C243	0.0000
C44	0.6525	C94	0.1877	C144	0.0520	C194	0.0154	C244	0.0000
C45	0.6936	C95	0.1826	C145	0.0507	C195	0.0151	C245	0.0000
C46	0.6744	C96	0.1777	C146	0.0494	C196	0.0148	C246	0.0000
C47	0.6560	C97	0.1730	C147	0.0482	C197	0.0144	C247	0.0000
C48	0.6384	C98	0.1684	C148	0.0470	C198	0.0141	C248	0.0000
C49	0.6214	C99	0.1640	C149	0.0458	C199	0.0139	C249	0.0000
C50	0.6204	C100	0.1597	C150	0.0447	C200	0.0136	C250	0.0000

Figure 5-99. Highly Dispersed Ruthenium Catalyst 4956-86 Conversions in Run 16 (H_2:CO Feed Ratio = 0.9, 208°C at Inlet, 35 atm)

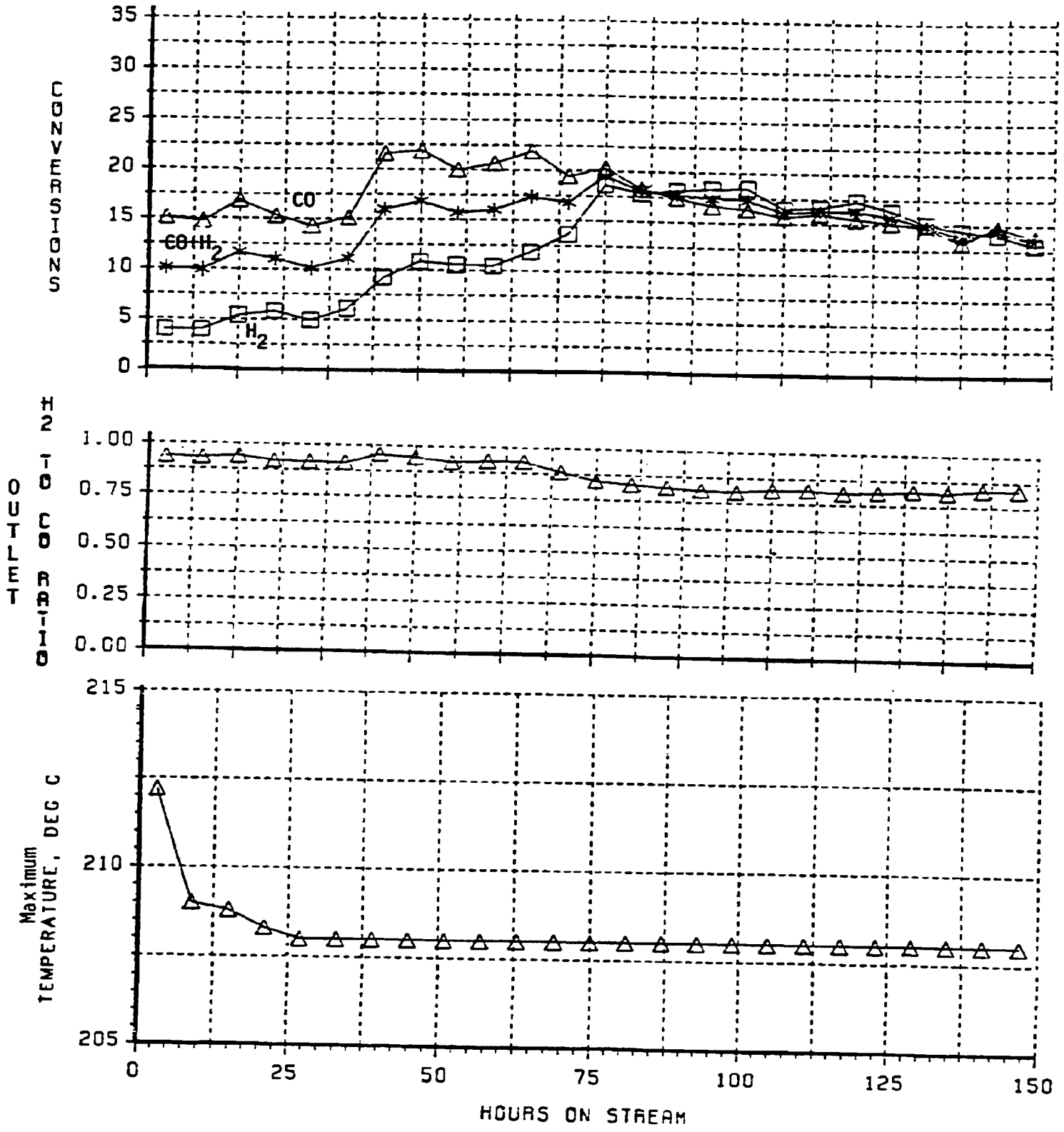

Figure 5-100. Highly Dispersed Ruthenium Catalyst 4956-86 Water Gas Shift Activity in Run 16 (H_2:CO Feed Ratio = 0.9, 208°C at Inlet, 35 atm)

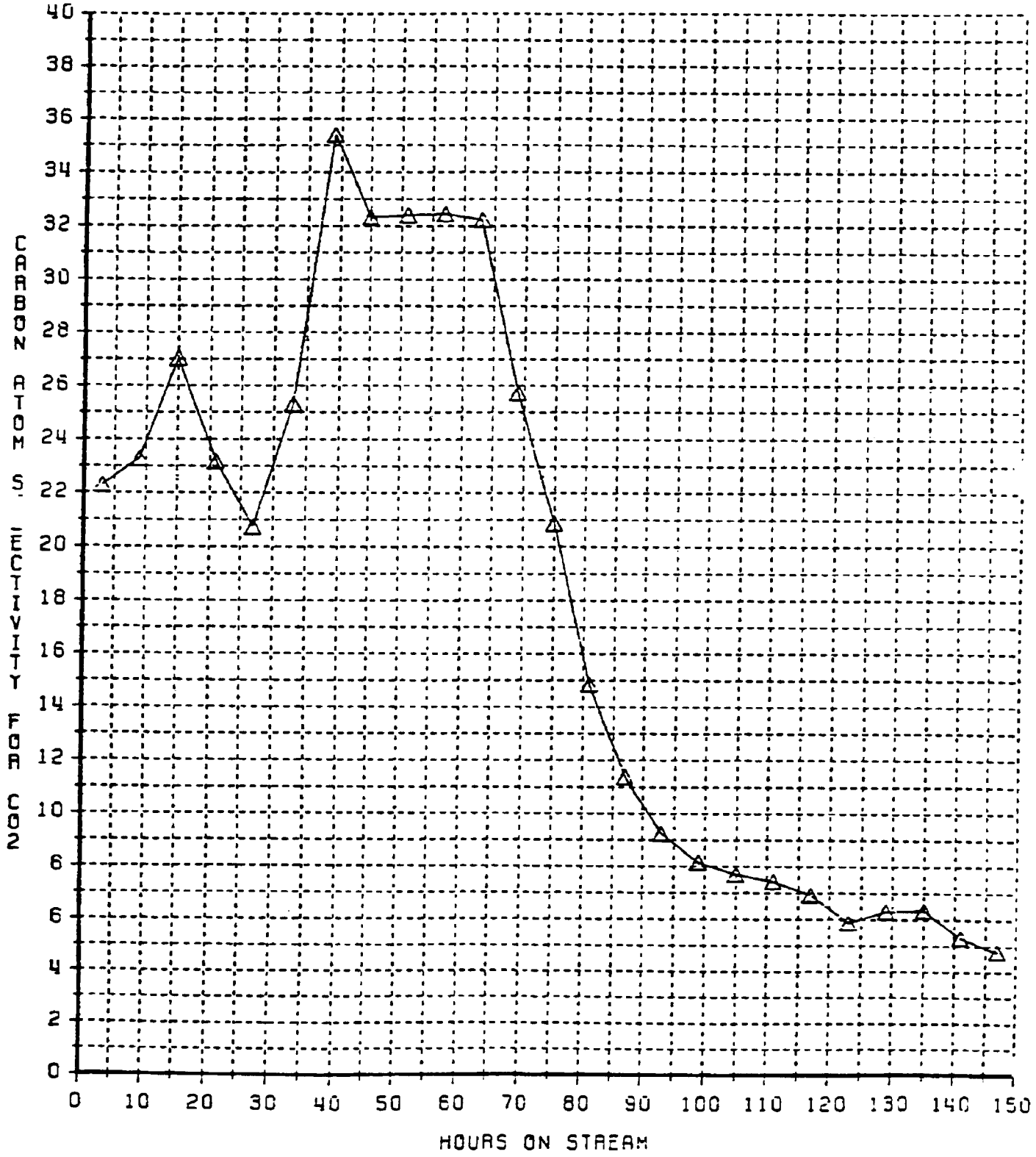

Figure 5-101. Highly Dispersed Ruthenium Catalyst 4956-86 C_1 and C_2 Selectivities in Run 16 (H_2:CO Feed Ration = 0.9, 208°C at Inlet, 35 atm)

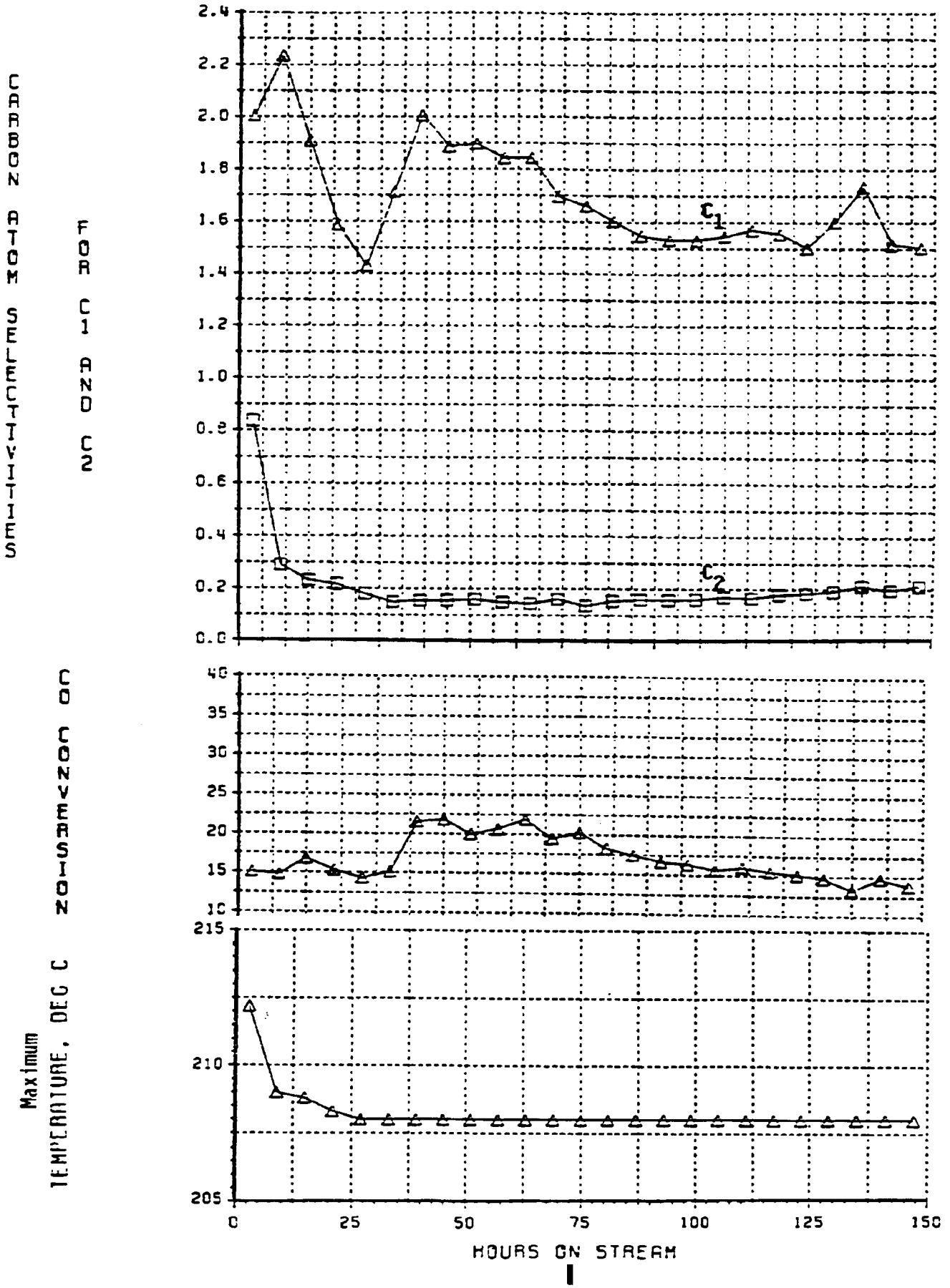

Figure 5-102. Highly Dispersed Ruthenium Catalyst 4956-86 C_3 and C_4 Selectivities in Run 16 (H_2:CO Feed Ratio = 0.9, 208°C at Inlet, 35 atm)

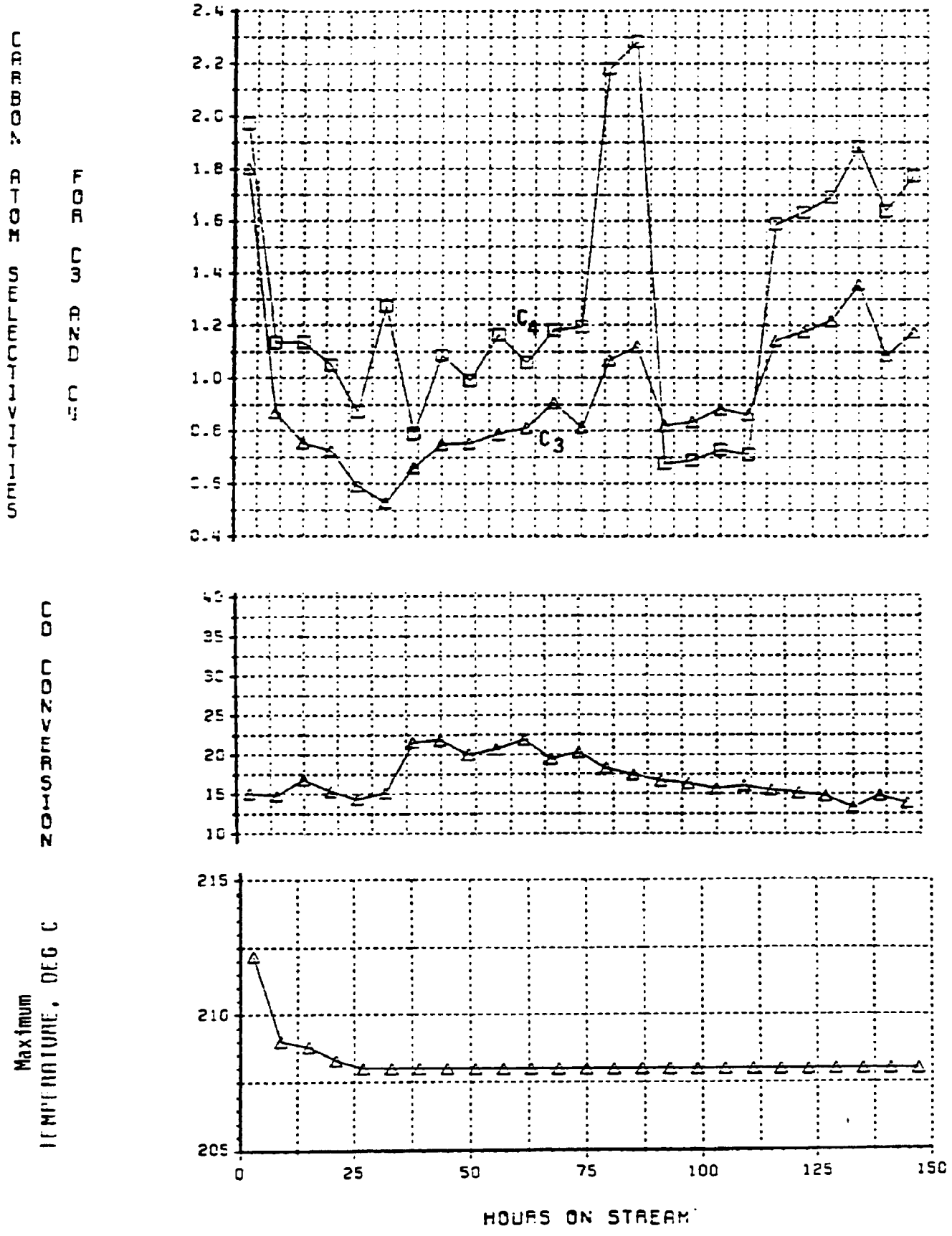

Figure 5-103. Highly Dispersed Catalyst 4956-86 Olefin to Paraffin Ratios in Run 16 (H_2:CO Feed Ratio = 0.9, 208°C at Inlet, 35 atm)

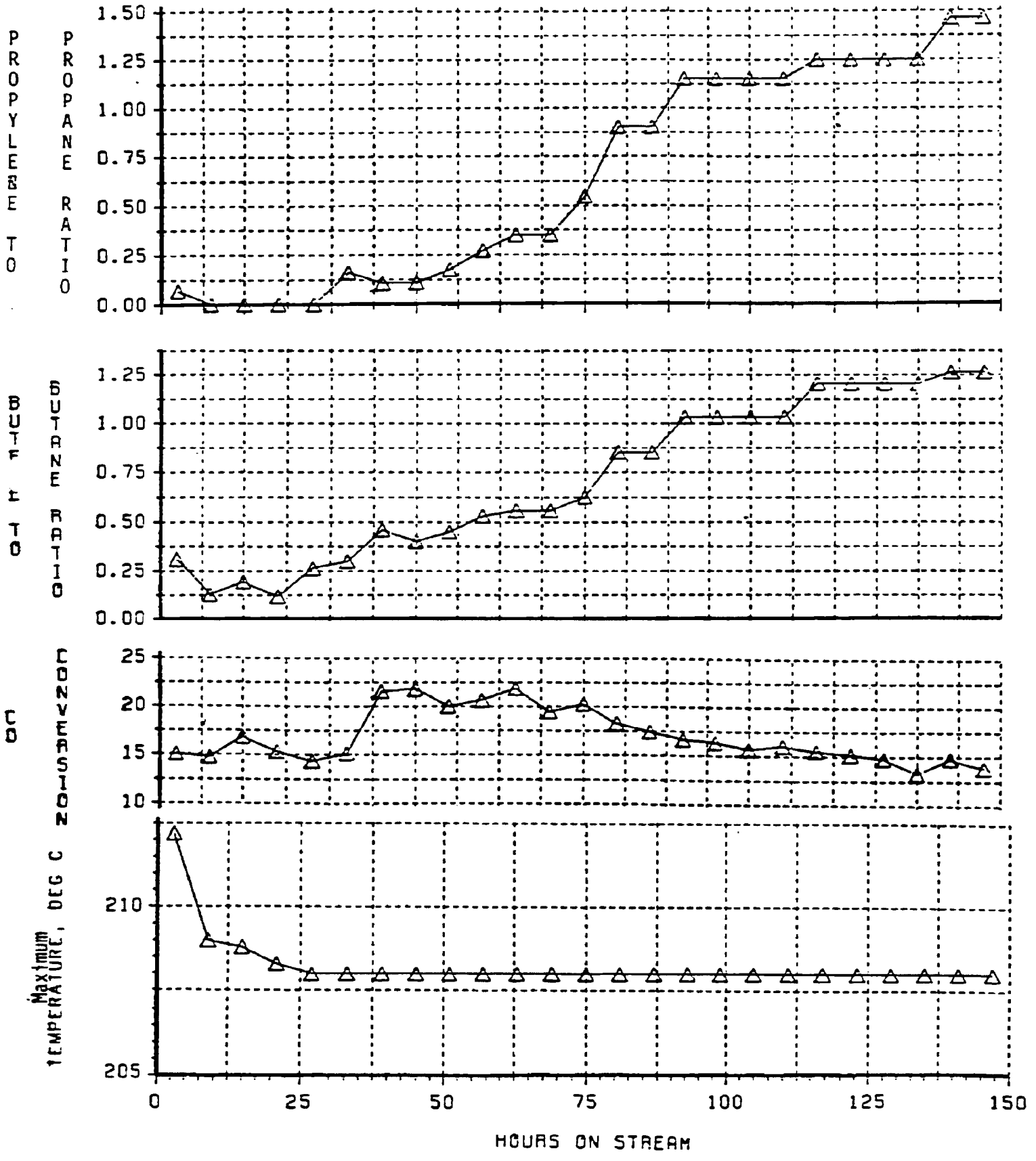

Figure 5-104. Gel Permeation Chromatography Analysis of Wax Extracted from Catalyst 4956-86 Used in Run 16

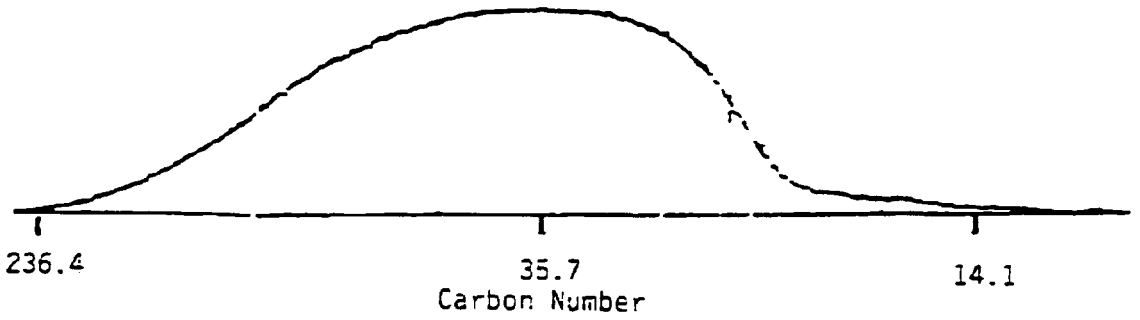

Figure 5-105. Anderson-Schulz-Flory Distribution with Highly Dispersed Ruthenium Catalyst 4956-86 in Run 16 (Hydrocarbons + Oxygenates)

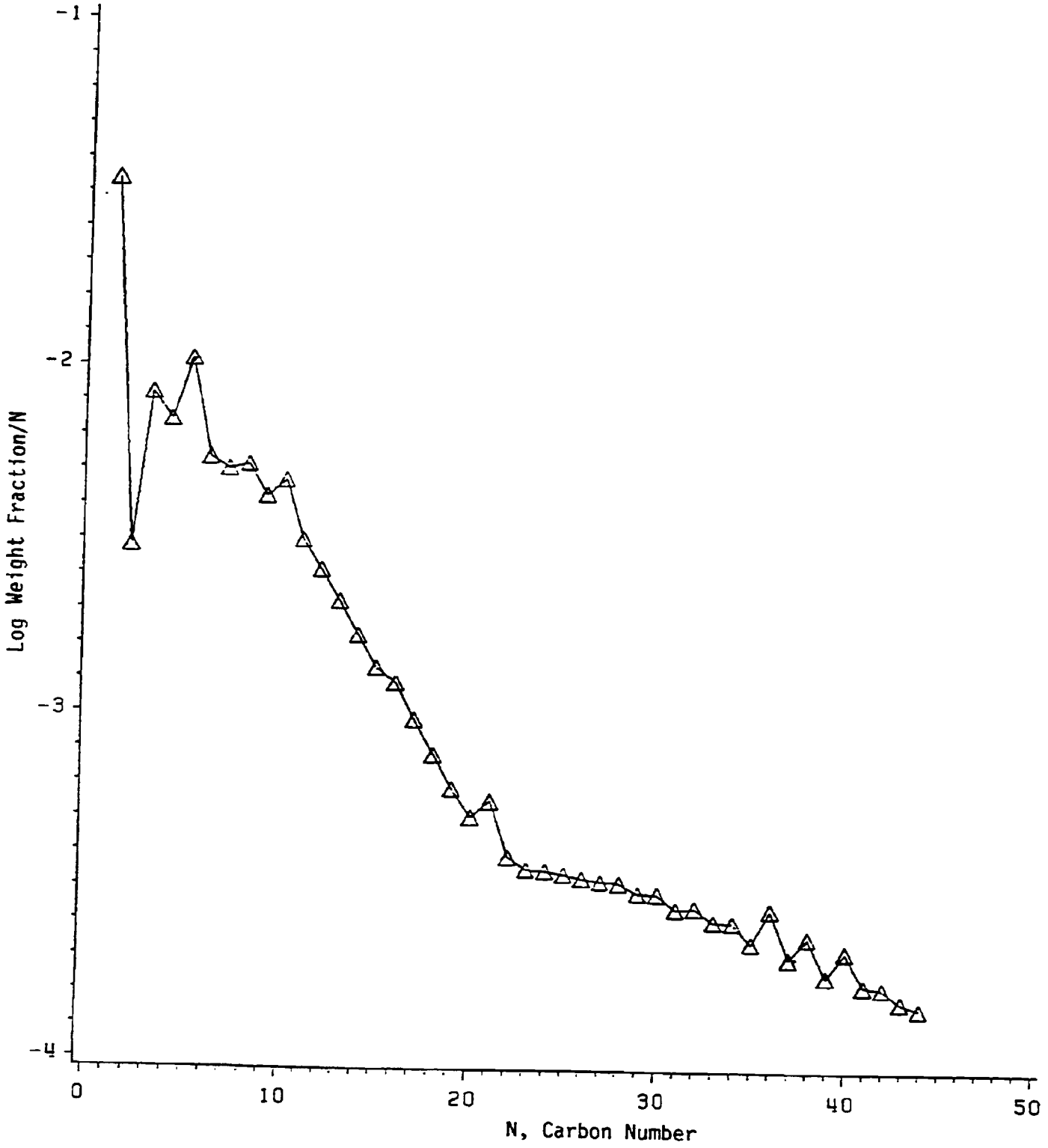

Figure 5-106. Anderson-Schulz-Flory Distribution with Highly Dispersed Ruthenium Catalyst 4956-86 in Run 16 (Hydrocarbons Only)

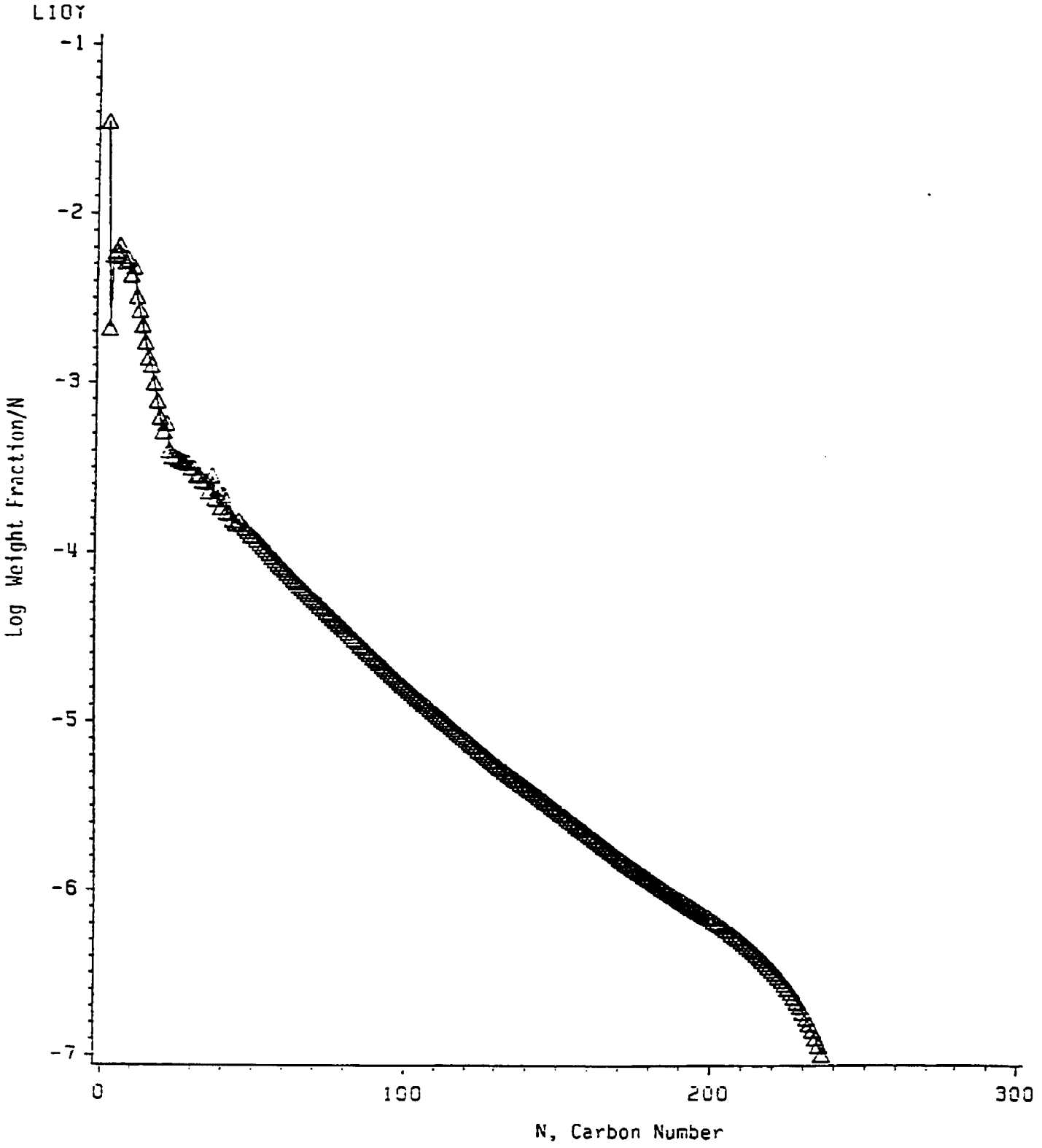

Analysis of the CO/H_2 reaction system in the appendix indicates that the source of CO_2 was probably the water gas shift reaction and not the Boudouard reaction ($2CO \rightarrow CO_2+C$). Accordingly, CO_2 formation throughout this work was tentatively attributed to the water gas shift reaction.

During the first 10 hours, the catalyst showed 22 to 27% carbon atom selectivity to CO_2, which later started to rapidly decrease (Figure 5-100). The decrease of the space velocity after 30 hours brought back the selectivity to CO_2 to about 35%. The selectivity to CO_2 increases with an increase in the overall conversion possibly because the water gas shift reaction occurs consecutive to the hydrocarbon synthesis reaction. After 60 hours, the selectivity to CO_2 started to rapidly decrease again. During the run, the CO_2 selectivity decreased much more rapidly than the $CO+H_2$ conversion, apparently indicating that the rate of the water gas shift reaction declined more rapidly than the rate of the hydrocarbon synthesis reaction.

Water gas shift activity was not previously reported for ruthenium Fischer-Tropsch catalysts. In view of the water gas shift reaction mechanism discussed in Section 2.2.1.4.2 these results may then suggest that part of the highly dispersed ruthenium on γ-Al_2O_3 may be in a positive oxidation state during Fischer-Tropsch synthesis.

The olefin to paraffin ratios gradually increased during the run from 0 to 1.45 at C_3 and from 0.1 to 1.25 at C_4 (Figure 5-103). C_2-C_4 products were made with selectivities below the Anderson-Schulz-Flory prediction (Figure 5-105). α was equal 0.832 for carbon number range C_1-C_{22}, 0.958 at C_{22}-C_{100} and 0.969 at C_{100}-C_{200} (Figures 5-105 and 5-106).

At the end of the run Catalyst 4956-86 was analyzed for ruthenium, which revealed that 43% of the ruthenium was lost from the catalyst in the 152-hour-test, apparently in the form of ruthenium carbonyl which was detected at the reactor outlet in the product receivers. Migration of ruthenium was also confirmed by STEM examination of the used catalyst, which indicated that a significant fraction of the alumina particles no longer contained ruthenium.